

A General Safety Framework for Autonomous Manipulation in Human Environments.

Jakob Thumm, Julian Balletshofer, Leonardo Maglanoc, Luis Muschal, and Matthias Althoff

Abstract—Autonomous robots are projected to augment the manual workforce, especially in repetitive and hazardous tasks. For a successful deployment of such robots in human environments, it is crucial to guarantee human safety. State-of-the-art approaches to ensure human safety are either too restrictive to permit a natural human-robot collaboration or make strong assumptions that do not hold when for autonomous robots, e.g., knowledge of a pre-defined trajectory. Therefore, we propose SaRA-shield, a power and force limiting framework for AI-based manipulation in human environments that gives formal safety guarantees while allowing for fast robot speeds. As recent studies have shown that unconstrained collisions allow for significantly higher contact forces than constrained collisions (clamping), we propose to classify contacts by their collision type using reachability analysis. We then verify that the kinetic energy of the robot is below pain and injury thresholds for the detected collision type of the respective human body part in contact. Our real-world experiments show that SaRA-shield can effectively reduce the speed of the robot to adhere to injury-preventing energy limits.

Index Terms—Human-robot collaboration, safety, power and force limiting, constrained contacts, clamping, reinforcement learning, artificial intelligence, speed and separation monitoring.

I. INTRODUCTION

Autonomous robots have already started to replace tedious, strenuous, and dangerous jobs [1, 2], and are projected to make up a relevant part of the future workforce [3, 4]. We expect these autonomous robots to be collaborative partners in our human world, which requires them to guarantee human safety while having a high level of interactivity. Previous approaches to ensure human safety in autonomous robotics often lack formal guarantees [5–10]. Most formal approaches, however, make assumptions that fail for fully autonomous robots, such as that robot paths are pre-defined to prevent human clamping [11, 12], that only contacts with the end effector are safety-critical [11, 13], or that the human is stationary [11]. Formal approaches that do not make these assumptions [14] are often too restrictive to enable a seamless human-robot collaboration (HRC).

ISO 10218-1 [15] and ISO/TS 15066 [16] define two possible forms of contact: *constrained contacts*, where the human is clamped by the robot link, and *unconstrained contacts*, where the human can freely move. Each contact comprises two phases: in the *transient* phase (first 0.5s), peak contact forces have to be limited to minimize the risk of injury; in

the subsequent *quasi-static* phase, clamping forces have to remain below the pain onset thresholds. The quasi-static phase is negligible for unconstrained contacts.

To mitigate the downsides of previous work, we propose SaRA-shield, a power and force limiting [15] approach for manipulators in human environments that gives formal safety guarantees for (a) dynamically changing robot paths, (b) full human-robot contact, and (c) dynamic human motion. As depicted in Fig. 1, in each control cycle, SaRA-shield determines the set of all possible states the human can occupy in a given time frame using a novel human motion model. It then uses reachability analysis to detect possible collisions between the robot and the human. We categorize the contact type into constrained and unconstrained contacts using the reachable sets of the human, the robot, and the environment. Once a contact is detected, we reduce the speed of the robot so that the kinetic energy of the robot link in contact is below the corresponding thresholds of the detected contact type. These thresholds have shown experimentally [15, 17, 18] to only cause minor skin injuries in the transient phase. By leveraging knowledge about the human pose in our model, we achieve higher speeds of the robot than previous power and force limiting approaches while giving stricter safety guarantees. As we base SaRA-shield on our previous work on provably safe manipulation for reinforcement learning-based HRC [19], we can directly deploy SaRA-shield on autonomous robots.

Our core contributions are

- a formal safety framework for manipulators in human environments including
- a reachability-based clamping detection, and
- an injury prevention based on admissible contact energies.

We claim that the kinetic energy of a robot controlled with SaRA-shield during a collision with a human is below thresholds that empirically exclude injuries.

This article is structured as follows: Sec. II discusses the related work. We then introduce the notation of our reachability analysis and the functionality of our previous safety shield in Sec. III. Sec. IV formally states the problem to solve. Sec. V gives a high-level overview of our proposed safety framework. We then discuss our proposed constrained collision detection in Sec. VI and our energy-based verification in Sec. VII. Finally, we evaluate our claims in Sec. VIII and give a conclusion and limitations of our work in Sec. IX.

II. RELATED WORK

This section will first introduce the notion of speed and separation monitoring and power and force limiting and discuss relevant methodologies implementing them. We will then

¹The authors are with the School of Informatics, Technical University of Munich, 85748 Garching, Germany. {jakob.thumm, julian.balletshofer, althoff}@tum.de

Manuscript received Month DD, YYYY; revised Month DD, YYYY.

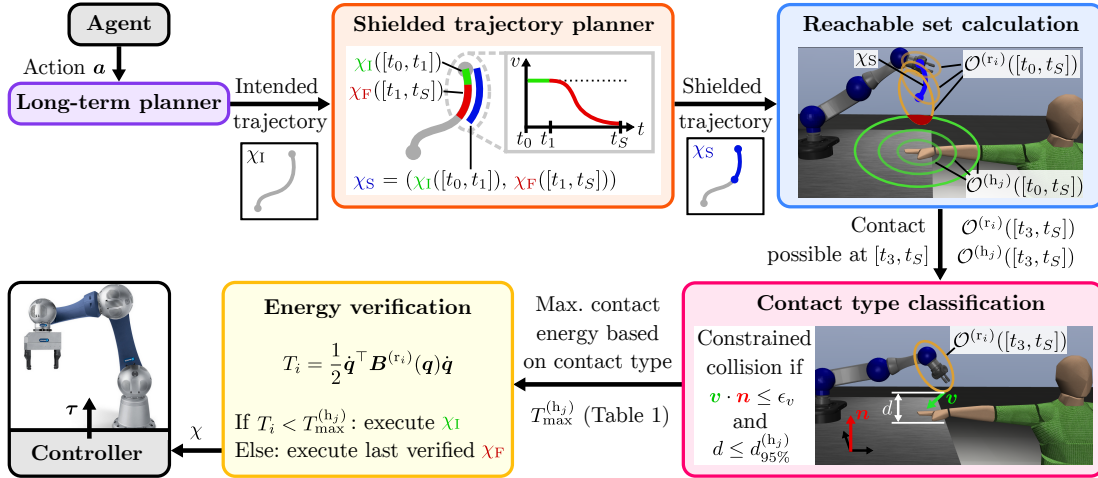


Fig. 1. Overview of the SaRA-shield safety framework. An action is translated into an intended trajectory. In each control cycle, SaRA shield calculates a shielded trajectory consisting of one time step intended trajectory followed by a failsafe trajectory. We check the shielded trajectory for possible human collisions using reachability analysis. When a possible contact with the human is detected, we classify the contact type into constrained and unconstrained collisions. We, finally, verify if the kinetic energy of the robot upon contact is below pain and injury limits for the given collision type. If the verification is safe, we execute the intended trajectory, and if it fails, we execute the last verified failsafe trajectory.

discuss recent human injury and pain onset studies and their implications for this work.

A. Speed and separation monitoring

In speed and separation monitoring [15], the robot is stopped before a human can reach it. Industrial applications usually implement speed and separation monitoring by enclosing the workspace of the robot with a light curtain that stops the robot once it is crossed. The safety distance between the robot and the human can be decreased when a variable braking time of the robot and a limited human velocity is assumed [20, 21]. When the human position can be continuously measured, the robot can resume its operation once the human retreats far enough from its workspace. The authors in [12, 19, 22–24] propose a formal speed and separation monitoring concept by over-approximating the reachable sets of the robot and the human. These approaches allow the robot to continue operation even if the human is relatively close (≈ 0.2 m), assuming measurements of the human pose are available.

B. Power and force limiting

In many HRC scenarios, we want to allow or even embrace contact with the human partner. ISO 10218-1 [15] permits such contacts using power and force limiting, where the robot is allowed to have a non-zero velocity at contact as long as transient and quasi-static force, pressure, or energy limits are not violated. It is important to note that not every body part can endure the same contact forces, as we discuss in Sec. II-C. Therefore, methods that do not assume knowledge about the human pose have to assume the worst case and tend to be restrictive in their maximal allowed velocity.

First approaches implementing power and force limiting proposed to stop the robot once a collision is detected based on an external force estimation from motor current differences [5, 6]. However, as shown in [25, 26], the reaction time

of such approaches is too slow to significantly mitigate the initial transient contact force spikes. Hence, these methods are only relevant for the quasi-static phase.

ISO/TS 15066 [16] defines a basic power and force limiting method that approximates the robot mass acting on the contact as half of the total robot mass and then calculates the maximal contact forces based on the kinetic energy of the robot. Although it is an easy-to-use model, Kirschner et al. [27] have shown that this robot mass calculation is incorrect, and the reflected robot mass [28] should be used instead.

Haddadin et al. [11] propose a power and force limiting approach based on this reflected robot mass, where they assume (a) knowledge of the human position, (b) that the human is stationary, and (c) the critical contact point is known. Using these assumptions, they determine the contact normal between the robot and the human, along which they calculate the reflected robot mass. Haddadin et al. [11] are also the first to propose the direct use of an injury database to determine a so-called safe motion unit, which returns the maximal allowed speed of the robot given a robot mass. They argue that this leads to a more accurate representation of the injury cases than the usually used transient force limits. Finally, they scale the speed of the robot to the maximal allowed value in each control cycle. The major downside of this approach is the assumed knowledge of the contact normal, which does not hold in reality.

To overcome this limitation, Steinecker et al. [10] propose to use the mean reflected mass over all possible contact normals as a mass metric. However, this is merely an approximation and cannot give formal safety guarantees. The authors in [14], therefore, propose not to calculate the reflected robot mass directly but to limit the total energy of the robot to a safe energy budget with a novel compliant controller. However, they do not take the human pose into account and thus have to use very restrictive energy thresholds.

A downside of most power and force limiting approaches [5,

6, 10, 11, 14, 29–33] is the assumption that contact is always possible, leading to a reduced speed of the robot even if the human is far away. To overcome this, the authors in [7, 8] propose to switch between power and force limiting and speed and separation monitoring based on the human distance. The approach in [12] extends this idea by dynamically reducing the speed of the robot if a possible contact is detected using reachability analysis. Liu and Althoff [13] further improve on this by replacing the otherwise fixed maximal contact velocity with a dynamic one that is verified using model conformance checking. Despite promising results, their approach is only applicable to end-effector contacts and requires human contact measurements for each new robot, body part, and a wide range of participants.

C. Human injuries

Human pain onset and skin damage depend on the impact energy, contact type, and contact shape [11, 34–37]. The most researched contact situations are constrained contacts with blunt impactors that evaluate the subjective onset of pain [36–39]. ISO/TS 15066 [16] defines force, pressure, and energy limits for constrained contacts, which seem to be confirmed by the aforementioned experimental studies. However, there remains a large variance in the study outcomes. When it comes to sharp or edged contacts in constrained contacts, the ex-vitro study of Kirschner et al. [17] shows that the ISO-defined limits are too high to prevent skin damage. A subsequent study for unconstrained collisions [18] showed that critical skin injuries occur at significantly higher impact velocities than in the constrained case. These studies highlight that possible contacts with sharp or edged robot areas have to be taken into account and that differentiation by contact case is beneficial for close interaction.

III. PRELIMINARIES

This section introduces our notation for reachability analysis and the safety shield concept we are building upon.

A. Reachability analysis

In this work, we adopt a reachability analysis approach for safety verification. Our considered systems follow the dynamics $\dot{\mathbf{x}}(t) = f(\mathbf{x}(t), \mathbf{u}(t), \mathbf{w}(t))$, with the state $\mathbf{x}(t) \in \mathbb{R}^n$, compact input set $\mathbf{u}(t) \in \mathcal{U} \subset \mathbb{R}^m$, compact disturbance set $\mathbf{w}(t) \in \mathcal{W} \subset \mathbb{R}^p$, and time $t \in \mathbb{R}_0^+$. The system admits a unique trajectory $\chi(t; \mathbf{x}_0, \mathbf{u}(\cdot), \mathbf{w}(\cdot)) \in \mathbb{R}^n$ for the given initial state \mathbf{x}_0 , input trajectory $\mathbf{u}(\cdot)$ ¹, and disturbance trajectory $\mathbf{w}(\cdot)$. The exact reachable set of the system at time t can be defined for a set of initial states \mathcal{X}_0 as

$$\mathcal{R}^e(t) = \{ \chi(t; \mathbf{x}_0, \mathbf{u}(\cdot), \mathbf{w}(\cdot)) \mid \mathbf{x}_0 \in \mathcal{X}_0, \forall \tau \in [t_0, t] : \mathbf{u}(\tau) \in \mathcal{U}, \mathbf{w}(\tau) \in \mathcal{W} \}. \quad (1)$$

If the input signal is generated by a state-feedback controller $\mathbf{u}_{\Phi_Z}(t) = \Phi_Z(\mathbf{x}(t))$, the resulting trajectory is denoted as

$\chi_Z(t; \mathbf{x}_0, \mathbf{u}_{\Phi_Z}(\cdot), \mathbf{w}(\cdot))$. The exact reachable set of a controlled system is then

$$\mathcal{R}_Z^e(t) = \{ \chi(t; \mathbf{x}_0, \mathbf{u}_{\Phi_Z}(\cdot), \mathbf{w}(\cdot)) \mid \mathbf{x}_0 \in \mathcal{X}_0, \forall \tau \in [t_0, t] : \mathbf{u}_{\Phi_Z}(\tau) = \Phi_Z(\mathbf{x}(\tau)), \mathbf{w}(\tau) \in \mathcal{W} \}. \quad (2)$$

In general, the exact reachable set $\mathcal{R}^e(t)$ cannot be computed, so we compute over-approximations for particular points in time $\mathcal{R}^e(t) \supseteq \mathcal{R}(t)$, which we simply refer to as reachable set in the future. All states reachable during the time interval $[t_0, t_f]$ are given by $\mathcal{R}([t_0, t_f]) = \bigcup_{t \in [t_0, t_f]} \mathcal{R}(t)$.

We denote the set of points that a system can occupy in Euclidean space at time t and the time interval $[t_0, t_f]$ as $\mathcal{O}(\mathcal{R}(t))$ and $\mathcal{O}(\mathcal{R}([t_0, t_f]))$, respectively, and further refer to it as reachable occupancy. Furthermore, we introduce a point in Euclidean space as \mathbf{p} , a ball with center \mathbf{c} and radius r as $\mathcal{B}(\mathbf{c}, r) = \{ \mathbf{p} \mid \|\mathbf{p} - \mathbf{c}\|_2 \leq r \}$, and a function that over-approximates a reachable occupancy with a ball $\mathcal{O} = \hat{\mathcal{B}}(\mathbf{c}, R)$ so that $\mathbf{p} \in \mathcal{O} \rightarrow \mathbf{p} \in \hat{\mathcal{B}}_{\mathcal{O}}$.

B. Safety shield

To ensure the safety of robots controlled by autonomous agents, we adapt the safety shield for manipulators proposed in [19]. The safety shield relies on the existence of a set of invariably safe states that can be reached from any state. Thumm and Althoff [19] define the set of invariably safe states as a fully stopped robot for manipulators in accordance with the speed and separation monitoring formulation in ISO 10218-1 2021 [15]. Thumm and Althoff [19] further demonstrated that a safety shield for autonomous agents is less restrictive when it operates on a higher frequency than the output frequency of the agent. They, therefore, execute each action of the agent \mathbf{a} for L time steps and perform a safety shield update at every time step.

At each time step k , the safety shield in [19] calculates an intended and a failsafe trajectory. Without loss of generality, we always reset the clock to $t_0 = 0$ at each time step. The intended trajectory χ_I follows the desired agent action output using the feedback controller $\Phi_I(\mathbf{x}(t), \mathbf{a})$ for L time steps. The failsafe trajectory χ_F leads the robot to an invariably safe state using a failsafe controller $\Phi_F(\mathbf{x}(t))$ in k_F time steps. The shield appends a full failsafe trajectory to a single step of the intended trajectory to form a so-called shielded trajectory

$$\chi_S = \begin{cases} \chi_I(t; \mathbf{x}_0, \mathbf{u}_{\Phi_I}(\cdot), \mathbf{w}(\cdot)), & t \in [t_0, t_D] \\ \chi_F(t; \mathbf{x}_D, \mathbf{u}_{\Phi_F}(\cdot), \mathbf{w}(\cdot)), & t \in [t_D, t_S], \end{cases} \quad (3)$$

with $D = 1$, t_S as the time of the end of the shielded trajectory, and $S = D + k_F$, as illustrated in the ‘‘Shielded trajectory planner’’ block of Fig. 1. Thumm and Althoff [19] verify the shielded trajectory by checking if it satisfies a collision constraint, as discussed in the next paragraph. If the verification fails, the shield safely executes the failsafe trajectory from the last successfully verified shielded trajectory. When assuming that the robot starts from an invariably safe state, safety can be ensured indefinitely by induction.

The authors in [12, 19] define the safety constraint for verification such that a collision between the human and robot

¹Note that $\mathbf{u}(\cdot)$ refers to the input trajectory and $\mathbf{u}(t)$ refers to the input at time t .

should be prevented entirely. For this, they calculate the reachable occupancies of all human body part parts $j = 1, \dots, J$ in the time interval $[t_0, t_S]$ as $\mathcal{O}^{(h)} = \bigcup_{j \in J} \mathcal{O}^{(h_j)}(\mathcal{R}^{(h_j)}([t_0, t_S]))$, where $\mathcal{R}^{(h_j)}([t_0, t_S])$ denotes the reachable set of the j -th human body part part assuming that the human inputs stem from a compact set $\mathbf{u}^{(h_j)}(t) \in \mathcal{U}^{(h_j)}$, e.g., each human body part part can have a maximal velocity of 1.6 m s^{-1} as defined in [40]. They further calculate the reachable occupancies of all robot links $i = 1, \dots, N$ in the time interval $[t_0, t_S]$ as $\mathcal{O}^{(r)} = \bigcup_{i \in N} \mathcal{O}^{(r_i)}(\mathcal{R}_S^{(r_i)}([t_0, t_S]))$, where $\mathcal{R}_S^{(r_i)}([t_0, t_S])$ denotes the reachable set of robot link i following the shielded trajectory. For the sake of readability, we abbreviate $\mathcal{O}^{(h_j)}(\mathcal{R}^{(h_j)}([t_0, t_f]))$ with $\mathcal{O}^{(h_j)}([t_0, t_f])$ and $\mathcal{O}^{(r_i)}(\mathcal{R}_S^{(r_i)}([t_0, t_f]))$ with $\mathcal{O}^{(r_i)}([t_0, t_f])$ in the future. The safety of the shielded trajectory can then be verified by checking if the reachable occupancies of the robot and the human are intersection-free using the constraint

$$\bar{c}_{\text{contact}}(\chi_S) := \mathcal{O}^{(r)} \cap \mathcal{O}^{(h)} = \emptyset. \quad (4)$$

Schepp et al. [24] enables an efficient computation of these reachable occupancies and intersection checks, using capsules as reachable occupancies of the robot links and human body parts. A capsule is defined by two end points $\mathbf{p}_1 \in \mathbb{R}^3$ and $\mathbf{p}_2 \in \mathbb{R}^3$ and a radius $r \in \mathbb{R}^+$ with $\mathcal{C}(\mathbf{p}_1, \mathbf{p}_2, r) = \overline{\mathbf{p}_1 \mathbf{p}_2} \oplus \mathcal{B}(\mathbf{0}, r)$, where $\overline{\mathbf{p}_1 \mathbf{p}_2}$ is the line segment between \mathbf{p}_1 and \mathbf{p}_2 , \oplus is the Minkowski sum, and $\mathbf{0}$ is the zero vector.

IV. PROBLEM STATEMENT

We aim to derive a safety framework that allows the robot to come into contact with the human as long as it is slow enough to prevent injuries. For this, we want to operate the robot at high speed as long as possible and only reduce the speed of the robot if necessary. ISO 10218-1 [15] provides three types of contact constraints: force, pressure, and energy, from which we are using the energy constraints for our problem statement. We define the compact set of goal states that follows from the action \mathbf{a} as $\mathcal{X}_g \subset \mathbb{R}^n$. Our objective is to minimize the time the robot needs to reach the goal while ensuring that if a contact with the human is possible, the robot energy is below human pain and injury limits with

$$\min_{\mathbf{u}_\Phi} t_g \quad (5a)$$

$$\text{subject to } \chi(t_g; \mathbf{x}_0, \mathbf{u}_\Phi(\cdot), \mathbf{w}(\cdot)) \in \mathcal{X}_g, \quad (5b)$$

$$\forall i, j, t: \mathcal{O}^{(h_j)}(t) \cap \mathcal{O}^{(r_i)}(t) = \emptyset \vee T^{(r_i)}(t) \leq T^{(h_j)}, \quad (5c)$$

$$i = 1, \dots, N, j = 1, \dots, J, t \in [t_0, t_g], \quad (5d)$$

$$\mathbf{u}^{(h_j)}(\cdot) \in \mathcal{U}^{(h_j)}, \mathbf{u}_\Phi(\cdot) \in \mathcal{U}, \mathbf{w}(\cdot) \in \mathcal{W}, \quad (5e)$$

where $T^{(r_i)}(t)$ describes the maximal reachable kinetic energy that robot link i induces into the human contact at time t and $T^{(h_j)}$ denotes the energy threshold of the j -th human body part. Note that the energy constraint can be converted into force or pressure constraints if we assume knowledge about the stiffness and damping properties of the human skin as detailed in ISO 10218-1 [15].

V. SAFETY FRAMEWORK FOR HUMAN-ROBOT INTERACTION

In this work, we adapt the safety shield approach of Thumm and Althoff [19] discussed in Sec. III-B to allow non-zero contact velocities. As highlighted in Sec. II-C, unconstrained contacts permit a significantly higher transient contact force than constrained contacts [17, 18]. Therefore, we first classify contacts into constrained and unconstrained contacts using reachability analysis. We then constrain the kinetic energy of the robot links at the contact points to be below the pain and injury limits for the respective contact type.

As the robot energy changes over the length of the shielded trajectory χ_S , we validate the contact constraints on shorter equidistant time intervals instead of the entire time interval $[t_0, t_S]$. Hence, we define our constraints on a trajectory χ_S for all time intervals, robot links, and human body parts

$$c_{\text{safe}}(\chi_S) := \bigwedge_{a=0}^{S-1} \bigwedge_{i=1}^N \bigwedge_{j=1}^J c_{\text{safe},i,j}([t_a, t_{a+1}]). \quad (6)$$

To improve readability, we give all constraints in the following sections for time intervals of length $\Delta t = t_1 - t_0$, but longer time intervals can be used to reduce computation time. The key idea of our verification is to define the safety constraint for a given robot link i , human body part j , and time interval $[t_0, t_1]$ as

$$c_{\text{safe},i,j}([t_0, t_1]) := \bar{c}_{\text{contact},i,j}([t_0, t_1]) \vee (c_{\text{free},i,j}([t_0, t_1]) \wedge c_{T, \text{free},i,j}) \vee (\bar{c}_{\text{free},i,j}([t_0, t_1]) \wedge c_{T, \text{clamp},i,j}), \quad (7)$$

where

- $\bar{c}_{\text{contact},i,j}$ evaluates if there is no contact between the robot link i and the human body part j ,
- $c_{\text{free},i,j}$ evaluates if the contact is an unconstrained collision,
- $c_{T, \text{free},i,j}$ evaluates if the kinetic energy of link i is below the injury threshold of body part j for unconstrained collisions, and
- $c_{T, \text{clamp},i,j}$ evaluates if the kinetic energy of link i is below the pain and injury threshold of body part j for constrained collisions.

We use the contact constraint between a robot link i , a human body part j , and a time interval $[t_0, t_1]$ from Liu and Althoff [13] as

$$\bar{c}_{\text{contact},i,j}([t_0, t_1]) := \mathcal{O}^{(h_j)}([t_0, t_1]) \cap \mathcal{O}^{(r_i)}([t_0, t_1]) = \emptyset. \quad (8)$$

We derive $c_{\text{free},i,j}$ in Sec. VI and $c_{T, \text{type},i,j}$ in Sec. VII.

Similar to Thumm and Althoff [19], we make two key assumptions in this work. First, we assume that the human pose is measurable with a bounded measurement error of δ_{meas} and a bounded time delay of Δt_{meas} . In our experiments, we achieve this by using a motion-tracking system, but our formulation can also be used with laser scanners [41] or depth cameras [42–45]. The measurement error and delay are incorporated into the human reachable set calculation using SaRA [24]. Second, we assume that a controller exists that tracks the desired trajectory with a bounded tracking

error, which is incorporated in the bounded system noise \mathcal{W} of the robot reachable occupancy calculation $\mathcal{O}^{(r)}$. In our experiments, we are using a simple PD-controller for trajectory tracking, but prior work has effectively demonstrated bounded tracking error guarantees for a trajectory tracking controller based on model conformance checking [46]. Similarly to most power and force limiting approaches [7, 8, 10–14, 29, 31–33], we also assume that the human does not actively move into hurtful contact with the robot so that the speed difference between the human and the robot along the contact normal is always smaller or equal to the robot speed. We do, however, take all possible human motion into account for contact detection and, therefore, do not assume the human to be static like Haddadin et al. [11]. In the following sections, we discuss how we can efficiently evaluate the constraint in (6).

VI. CONSTRAINED COLLISION DETECTION

In this section, we present how we can use reachability analysis to detect potential constrained collisions. In general, the human can be clamped between the robot and the static environment or between two robot links. We will refer to these two cases as environmentally-constrained collisions (ECCs) and self-constrained collisions (SCCs). Hence, we can ensure that a collision between link i and body part j in the time interval $[t_0, t_1]$ is unconstrained if

$$c_{\text{free},i,j}([t_0, t_1]) := \bar{c}_{\text{ECC},i,j}([t_0, t_1]) \wedge \bar{c}_{\text{SCC},i,j}([t_0, t_1]). \quad (9)$$

In the following subsections, we will derive the general constraints $\bar{c}_{\text{ECC},i,j}$ and $\bar{c}_{\text{SCC},i,j}$, formulate a series of relaxations of those constraints, and discuss how we handle clamping of multiple human body parts at the same time.

A. General ECC and SCC constraints

For detecting ECCs, we assume there is an over-approximating time-independent compact set representation of all environment elements that can cause clamping. This information is typically available in industrial applications or can be obtained using 3D laser scanning [47]. Making this assumption, we can model the environment as a composition of K large unmovable elements, such as walls, the floor, or a table, with time-independent reachable occupancies $\mathcal{O}^{(e_k)}$, $k = 1, \dots, K$. We define a trajectory χ_S to be free of ECCs between a link i and a body part j in a time interval $[t_0, t_1]$ if:

$$\bar{c}_{\text{ECC},i,j}([t_0, t_1]) := \bigwedge_{k=1}^K \bar{c}_{\text{ECC},i,j,k}([t_0, t_1]) \quad (10)$$

$$\bar{c}_{\text{ECC},i,j,k}([t_0, t_1]) := \mathcal{O}^{(h_j)}([t_0, t_1]) \cap \mathcal{O}^{(e_k)} = \emptyset, \quad (11)$$

i.e., there cannot be an ECC with environment element k if the human occupancy does not intersect with the reachable occupancy of the environment element.

For SCCs, we exclude a potential clamping of a human body part j between two robot links $i = 1, \dots, N$ and $l = 1, \dots, N$, with $i \neq l$ in a time interval $[t_0, t_1]$ if:

$$\bar{c}_{\text{SCC},i,j,l}([t_0, t_1]) := \bar{c}_{\text{contact},l,j}([t_0, t_1]), \quad (12)$$

i.e., there cannot be an SCC if the human occupancy does not intersect with two different robot links. Note that a possible contact between the link i and the body part j is already a prerequisite for any collision type according to (7). Based on (12), we define the SCC constraint for a link i and a body part j as

$$\bar{c}_{\text{SCC},i,j}([t_0, t_1]) := \bigwedge_{l=1}^N l \neq i \vee \bar{c}_{\text{SCC},i,j,l}([t_0, t_1]). \quad (13)$$

B. Reducing restrictiveness

The constraints in (10) and (13) are quite restrictive and would be violated in most close HRC. Therefore, we propose three adaptations that reduce the restrictiveness of these constraints using prior knowledge of the robot trajectory and human embodiments.

1) *Robot velocity*: We can use the knowledge of the robot trajectory to deduce a set of exceptions in which clamping is impossible. In the ECC case, clamping of a human body part by a robot link can only occur if the robot link is moving in the direction of the environment element. Likewise, SCCs require the two robot links to move towards each other.

For a potential ECC between link i , body part j , and environment element k , we first determine if the two reachable occupancies $\mathcal{O}^{(r_i)}([t_0, t_1])$ and $\mathcal{O}^{(e_k)}$ intersect. If so, we assume that clamping is possible. Otherwise, we determine the pair of closest points between the reachable occupancies $\mathcal{O}^{(r_i)}([t_0, t_1])$ and $\mathcal{O}^{(e_k)}$ using

$$\hat{\mathbf{p}}^{(r_i)}, \hat{\mathbf{p}}^{(e_k)} = \arg \min_{\mathbf{p}^{(r_i)}, \mathbf{p}^{(e_k)}} \|\mathbf{p}^{(r_i)} - \mathbf{p}^{(e_k)}\|_2 \quad (14)$$

$$\text{subject to } \mathbf{p}^{(r_i)} \in \mathcal{O}^{(r_i)}([t_0, t_1]), \mathbf{p}^{(e_k)} \in \mathcal{O}^{(e_k)}.$$

We then determine the normal $\mathbf{n}^{(e_k)}$ on $\mathcal{O}^{(e_k)}$ at $\hat{\mathbf{p}}^{(e_k)}$. We define the reachable velocity of the robot link i in the time interval $[t_0, t_1]$ as $\mathcal{V}^{(r_i)}([t_0, t_1]) = v(\mathcal{R}_S^{(r_i)}([t_0, t_1]))$, where $v: \mathcal{P}(\mathbb{R}^n) \rightarrow \mathcal{P}(\mathbb{R}^3)$ extracts all possible linear velocities from a reachable set and \mathcal{P} is the power set. Using the velocity information, a constrained collision involving the robot link i and another object with contact normal \mathbf{n} in the time interval $[t_0, t_1]$ can be excluded if

$$\forall \hat{\mathbf{p}}^{(r_i)} \in \mathcal{V}^{(r_i)}([t_0, t_1]) : \dot{\hat{\mathbf{p}}}^{(r_i)} \cdot \mathbf{n} \geq 0, \quad (15)$$

where \cdot is the dot product, i.e., all points on the robot link are moving in the direction of the normal vector \mathbf{n} . In the following paragraph, we present how we efficiently evaluate (15) in practice.

a) *Calculation of the reachable velocity*: In SaRA-shield, we use capsules to represent the reachable occupancies of the robot links as described in Sec. III-B. We denote the linear and angular velocity of a point \mathbf{p} as $\mathbf{v} = [\dot{\mathbf{p}}, \boldsymbol{\omega}]^\top$.

Theorem VI.1. *All points in a capsule $\mathcal{C}(\mathbf{p}_1, \mathbf{p}_2, r)$ with $\mathbf{v}_1 = [\dot{\mathbf{p}}_1, \boldsymbol{\omega}_1]^\top$ are moving away from an object with normal vector \mathbf{n} if*

$$\mathbf{n} \cdot \dot{\mathbf{p}}_1 + (r + \|\mathbf{p}_2 - \mathbf{p}_1\|_2) \|\mathbf{n} \times \boldsymbol{\omega}_1\|_2 > 0. \quad (16)$$

Proof. Let the set of linear velocities of all points in a capsule be denoted as $\mathcal{V} = \{\dot{\mathbf{p}} \mid \mathbf{p} \in \mathcal{C}(\mathbf{p}_1, \mathbf{p}_2, r)\}$. Given a vector \mathbf{n} ,

we want to determine the minimal speed any point in a capsule \mathcal{C} has in the direction of \mathbf{n} as

$$\check{v}_{\mathbf{n}} = \min_{\dot{\mathbf{p}}} \mathbf{n} \cdot \dot{\mathbf{p}} \quad (17)$$

subject to $\dot{\mathbf{p}} \in \mathcal{V}$.

A point in the capsule $\mathcal{C}(\mathbf{p}_1, \mathbf{p}_2, r)$ can be described as $\mathbf{p}_c = \mathbf{p}_1 + \lambda \mathbf{d} + \mathbf{r}$, where $\mathbf{d} = \mathbf{p}_2 - \mathbf{p}_1$, $\lambda \in [0, 1]$, and $\|\mathbf{r}\|_2 \leq r$. The velocity of such a point is

$$\dot{\mathbf{p}}_c = \dot{\mathbf{p}}_1 + \boldsymbol{\omega}_1 \times \mathbf{p}_c \quad (18)$$

$$= \dot{\mathbf{p}}_1 + \boldsymbol{\omega}_1 \times \mathbf{r} + \lambda \boldsymbol{\omega}_1 \times \mathbf{d}, \quad (19)$$

and its speed along a vector \mathbf{n} is

$$\mathbf{n} \cdot \dot{\mathbf{p}}_c = \mathbf{n} \cdot \dot{\mathbf{p}}_1 + \mathbf{n} \cdot (\boldsymbol{\omega}_1 \times \mathbf{r}) + \lambda \mathbf{n} \cdot (\boldsymbol{\omega}_1 \times \mathbf{d}) \quad (20)$$

$$= \mathbf{n} \cdot \dot{\mathbf{p}}_1 + \|\mathbf{r} + \lambda \mathbf{d}\|_2 \|\mathbf{n} \times \boldsymbol{\omega}_1\|_2 \cos(\alpha), \quad (21)$$

where α is the angle between $\mathbf{r} + \lambda \mathbf{d}$ and $\mathbf{n} \times \boldsymbol{\omega}_1$. We derive the lower limit of this speed as

$$\mathbf{n} \cdot \dot{\mathbf{p}}_c \geq \mathbf{n} \cdot \dot{\mathbf{p}}_1 + \|\mathbf{r} + \lambda \mathbf{d}\|_2 \|\mathbf{n} \times \boldsymbol{\omega}_1\|_2 \quad (22)$$

$$\geq \mathbf{n} \cdot \dot{\mathbf{p}}_1 + (r + \lambda \|\mathbf{d}\|_2) \|\mathbf{n} \times \boldsymbol{\omega}_1\|_2 \quad (23)$$

$$\geq \mathbf{n} \cdot \dot{\mathbf{p}}_1 + (r + \|\mathbf{d}\|_2) \|\mathbf{n} \times \boldsymbol{\omega}_1\|_2 = \check{v}_{\mathbf{n}}. \quad (24)$$

Therefore, all points on a capsule $\mathcal{C}(\mathbf{p}_1, \mathbf{p}_2, r)$ move away from an object with normal vector \mathbf{n} if $\check{v}_{\mathbf{n}} > 0$. \square

We use the link Jacobian [48, Eq. 7.16] to calculate the velocity of point $\mathbf{p}_1^{(r_i)}(t)$ as $\mathbf{v}_1^{(r_i)}(t) = \mathbf{J}^{(r_i)}(\mathbf{q}(t))\dot{\mathbf{q}}(t)$. We then assume that $\check{v}_{\mathbf{n}}$ evolves linearly between two time points, so that we can determine the maximal speed a link can have in the direction of \mathbf{n} in the time interval $[t_0, t_1]$ as

$$\check{v}_{\mathbf{n}}^{(r_i)} = \min(\mathbf{n} \cdot \dot{\mathbf{p}}_1^{(r_i)}(t_0) + (r^{(r_i)} + d^{(r_i)}) \|\mathbf{n} \times \boldsymbol{\omega}_1^{(r_i)}(t_0)\|_2, \mathbf{n} \cdot \dot{\mathbf{p}}_1^{(r_i)}(t_1) + (r^{(r_i)} + d^{(r_i)}) \|\mathbf{n} \times \boldsymbol{\omega}_1^{(r_i)}(t_1)\|_2), \quad (25)$$

where $r^{(r_i)}$ and $d^{(r_i)} = \|\mathbf{p}_2^{(r_i)} - \mathbf{p}_1^{(r_i)}\|_2$ are the radius and length of the i -th robot capsule. We account for the linearization error ϵ_v between two time points by evaluating

$$\check{v}_{\mathbf{n}}^{(r_i)} \geq \epsilon_v. \quad (26)$$

Theorem VI.2. *The linearization error of the linear velocity $\dot{\mathbf{p}}$ projected onto an vector \mathbf{n} of an arbitrary point \mathbf{p} on the robot in the time interval $t \in [t_0, t_0 + \Delta t]$ is bounded by*

$$\epsilon_v = \frac{\Delta t}{8} \sum_{k=1}^N \sum_{i=k}^N d_i \left[\ddot{q}_{k,max} + \ddot{q}_{k,max} \sum_{j=1}^i \dot{q}_{j,max} + \dot{q}_{k,max} \left(\sum_{j=1}^i \ddot{q}_{j,max} + \left(\sum_{j=1}^i \dot{q}_{j,max} \right)^2 \right) \right], \quad (27)$$

where $\dot{q}_{k,max}$, $\ddot{q}_{k,max}$, and $\ddot{q}_{k,max}$ are the maximal allowed joint velocity, acceleration, and jerk over all trajectories and for all times t with

$$\dot{q}_{k,max} = \sup_{t \leq \tau \leq t + \Delta t} |\dot{q}_k(\tau)| \quad (28)$$

$$\ddot{q}_{k,max} = \sup_{t \leq \tau \leq t + \Delta t} |\ddot{q}_k(\tau)| \quad (29)$$

$$\ddot{q}_{k,max} = \sup_{t \leq \tau \leq t + \Delta t} |\ddot{q}_k(\tau)|. \quad (30)$$

We give the proof for Theorem VI.2 in Appendix Sec. A.

b) Velocity constraints: With (26), we can re-define the ECC constraint in (10) to exclude cases, where the robot is moving away from the environment element, using

$$\check{c}_{\text{ECC},i,j,k}^{\prime}([t_0, t_1]) := \bar{c}_{\text{ECC},i,j,k}([t_0, t_1]) \vee (\check{v}_{\mathbf{n}}^{(r_i)} \geq \epsilon_v). \quad (31)$$

Similar to the ECC case, we can re-define the SCC constraint in (13) to exclude cases, where the two robot links move away from each other, using

$$\check{c}_{\text{SCC},i,j,l}^{\prime}([t_0, t_1]) := \bar{c}_{\text{SCC},i,j,l} \vee (\check{v}_{\mathbf{n}_l}^{(r_i)} \geq \check{v}_{\mathbf{n}_l}^{(r_i)} + \epsilon_v), \quad (32)$$

where the vector \mathbf{n}_l is the normal vector on robot link l for the closest point between the two reachable occupancies $\mathcal{O}^{(r_i)}([t_0, t_1])$ and $\mathcal{O}^{(r_i)}([t_0, t_1])$, which we determine analogously to (14).

2) Human diameter: Another natural condition that is required for constrained collisions is that the distance between the robot link and environment element (ECC) or the two robot links (SCC) must be smaller or equal to the maximal diameter of the human body part that could be clamped. Therefore, we extend the constraints in (31) to

$$\check{c}_{\text{ECC},i,j,k}^{\prime\prime}([t_0, t_1]) := \check{c}_{\text{ECC},i,j,k}^{\prime}([t_0, t_1]) \vee \text{dist}(\mathcal{O}^{(r_i)}([t_0, t_1]), \mathcal{O}^{(\epsilon_k)}) > 2r^{(h_j)}, \quad (33)$$

and the one in (32) to

$$\check{c}_{\text{SCC},i,j,l}^{\prime\prime}([t_0, t_1]) := \check{c}_{\text{SCC},i,j,l}^{\prime}([t_0, t_1]) \vee \text{dist}(\mathcal{O}^{(r_i)}([t_0, t_1]), \mathcal{O}^{(r_i)}([t_0, t_1])) \leq 2r^{(h_j)}, \quad (34)$$

where dist is a distance function that measures the smallest distance between two sets and $r^{(h_j)}$ is the radius of the human body part. In Euclidean space, the distance function can be described as

$$\text{dist}(\mathcal{S}_1, \mathcal{S}_2) = \inf_{\mathbf{p}_1, \mathbf{p}_2} \|\mathbf{p}_1 - \mathbf{p}_2\|_2, \mathbf{p}_1 \in \mathcal{S}_1, \mathbf{p}_2 \in \mathcal{S}_2, \quad (35)$$

which we can efficiently calculate for capsule representations using SaRA [24]. In SaRA-shield, we use the 95 percentile information about the dimension of human body parts defined in DIN 33402-2:2020-12 [49] as an upper bound for the diameters of human body parts. We assume that the system is informed if a particularly large human operates next to the robot.

3) Robot topology: Most collaborative robots are designed to prevent clamping between certain robot links, either through their topology or by the joint angle limits. Hence, for a given robot, we define the set of robot occupancy pairs that cannot cause an SCC as

$$\mathcal{G}^{(r)} = \{(i, l) \mid \text{no SCC between link } i \text{ and } l \text{ possible}\} \quad (36)$$

and extend (34) with

$$\check{c}_{\text{SCC},i,j,l}^{\prime\prime\prime}([t_0, t_1]) := \check{c}_{\text{SCC},i,j,l}^{\prime\prime}([t_0, t_1]) \vee (i, l) \in \mathcal{G}^{(r)}. \quad (37)$$

4) Full constrained collision detection: With the derived constraint relaxations, we redefine the unconstrained collision constraint in (9) as

$$c_{\text{free},i,j}^{\prime\prime\prime}([t_0, t_1]) := \bigwedge_{k=1}^K \check{c}_{\text{ECC},i,j,k}^{\prime\prime\prime}([t_0, t_1]) \wedge \bigwedge_{l=1}^N l \neq i \vee \check{c}_{\text{SCC},i,j,l}^{\prime\prime\prime}([t_0, t_1]). \quad (38)$$

C. Handling Multi-Body Clamping

An important scenario to consider is the case where the robot clamps multiple human body parts, e.g., both hands are clamped in between the robot and a table. In these cases, the constraint in (38) does not guarantee the detection of all possible constrained contacts anymore. To handle the clamping of multiple human body parts at the same time, we first find all body parts that are connected and could be part of a constrained collision and combine them into a new virtual body part. Fortunately, there are a number of human body part combinations that cannot lead to critical constrained collision and can thereby be excluded, e.g., multiple body parts from the same extremity. Therefore, we define the set of safe body part pairs as

$$\mathcal{G}^{(h)} = \{(j, j') \mid \text{no clamping of body part } j \text{ and } j' \text{ possible}\}. \quad (39)$$

To efficiently find ECCs and SCCs, we construct an undirected graph, where the vertices are the robot links, human body parts, and environment elements, denoted as r_i , h_j , and e_k . The edges between two vertices n_1 and n_2 are denoted as $\{n_1, n_2\}$. We construct an edge

$$\{r_i, h_j\} \text{ if } \mathcal{O}^{(h_j)} \cap \mathcal{O}^{(r_i)} \neq \emptyset \quad (40)$$

$$\{h_j, e_k\} \text{ if } \mathcal{O}^{(h_j)} \cap \mathcal{O}^{(e_k)} \neq \emptyset \quad (41)$$

$$\{h_j, h_{j'}\} \text{ if } \mathcal{O}^{(h_j)} \cap \mathcal{O}^{(h_{j'})} \neq \emptyset \wedge (j, j') \notin \mathcal{G}^{(h)} \quad (42)$$

$$\{r_i, r_l\} \text{ if } i \neq l \wedge (i, l) \notin \mathcal{G}^{(r)} \quad (43)$$

A path through the graph gives rise to the vertex sequence $\{n_1, n_2, \dots, n_n\}$. The robot link i can then cause a combined ECC of M human body parts $h_{j,1}, \dots, h_{j,M}$ on the environment element k if there exists a vertex sequence $\{r_i, n_2, \dots, n_{M+1}, e_k\}$, where n_2, \dots, n_{M+1} is any permutation of $h_{j,1}, \dots, h_{j,M}$. Similarly, a possible combined SCC between robot links i and l exists if there is a vertex sequence $\{r_i, r_l, n_2, \dots, n_{M+1}, r_i\}$, where n_2, \dots, n_{M+1} is any permutation of $h_{j,1}, \dots, h_{j,M}$. To find both combined ECCs and SCCs, we conduct a depth-first search graph coloring algorithm. Since multi-body part contacts are more restrictive than single-body part contacts, we always start the search at a human body part h_j and move along the edges $\{h_j, h_{j'}\}$ first. For all combined ECCs and SCCs, we combine the human body parts $h_{j,1}, \dots, h_{j,M}$ to new virtual body parts \tilde{j} with a combined radius of $r^{(h_{\tilde{j}})} = r^{(h_{j,1})} + \dots + r^{(h_{j,M})}$ and an occupancy of $\mathcal{O}^{(h_{\tilde{j}})} = \mathcal{O}^{(h_{j,1})} \cup \dots \cup \mathcal{O}^{(h_{j,M})}$. This leads to an increase in the number of human body parts from J to \tilde{J} , which we use to update the constraint in (6) by replacing J with \tilde{J} .

VII. CONTACT ENERGY CONSTRAINTS

In this section, we discuss how we evaluate the contact energy constraints $c_{T, \text{free}, i, j}$ and $c_{T, \text{clamp}, i, j}$ in (6). For this, we derive the kinetic energy of a robot link i in a given configuration and define the necessary constraints for all possible contacts.

The kinetic energy of the entire robot is [48]

$$T(\mathbf{q}) = \frac{1}{2} \dot{\mathbf{q}}^\top \mathbf{B}(\mathbf{q}) \dot{\mathbf{q}}, \quad (44)$$

where $\mathbf{B}(\mathbf{q})$ is the inertia matrix. In this work, we assume that the robot consists of rigid body parts without joint elasticity, where the motor masses and inertia are included in the links, so we can formulate the inertia matrix as [48, Eq. 7.32]

$$\mathbf{B}(\mathbf{q}) = \sum_{i=1}^N m_{\ell_i} \mathbf{J}_P^{(\ell_i)\top} \mathbf{J}_P^{(\ell_i)} + \mathbf{J}_O^{(\ell_i)\top} \mathbf{R}_i \mathbf{I}_{\ell_i}^i \mathbf{R}_i^\top \mathbf{J}_O^{(\ell_i)}, \quad (45)$$

where m_{ℓ_i} is the mass of link i , $\mathbf{J}_P^{(\ell_i)}$ and $\mathbf{J}_O^{(\ell_i)}$ are the link Jacobian of link i [48, Eq. 7.16] with respect to the position and orientation, \mathbf{R}_i is the rotation matrix from the i -th link frame to the base frame, and $\mathbf{I}_{\ell_i}^i$ is the inertia tensor of link i . When determining the maximal possible contact energy of a robot link $i < N$, we can ignore the energy induced by the rotation around the joints $i+1, \dots, N$. As a simple example, take a six degree of freedom robot for which only the last joint has a non-zero velocity. Here, any contact with links one to five would exert zero energy on the human body part, and only a contact with the last link would have a non-zero energy. The maximal kinetic energy exerted by a contact with robot link i is then

$$T_i(\mathbf{q}) = \frac{1}{2} \dot{\mathbf{q}}^\top \mathbf{E}_i \mathbf{B}(\mathbf{q}) \mathbf{E}_i \dot{\mathbf{q}}. \quad (46)$$

where \mathbf{E}_i is the truncated identity matrix with 1s on the diagonal up to row i and 0s elsewhere. In other words, we set the velocity of the robot joints $i+1, \dots, N$ to zero.

We can now define the contact energy constraints in (6) as

$$c_{T, \text{free}, i, j}([t_0, t_1]) = \max(T_i(\mathbf{q}(t_0)), T_i(\mathbf{q}(t_1))) < T_{\text{free}, i}^{(h_j)} \quad (47)$$

$$c_{T, \text{clamp}, i, j}([t_0, t_1]) = \max(T_i(\mathbf{q}(t_0)), T_i(\mathbf{q}(t_1))) < T_{\text{clamp}, i}^{(h_j)} \quad (48)$$

where $T_{\text{type}, i}^{(h_j)}$ gives the maximal contact energy for the respective human body part, contact type, and link index as listed in Table I. The link index is included in this threshold so that we can differentiate between different worst-case contact shapes on the different links. For most collaborative robots the first $N-1$ links are designed to only induce blunt contacts, whereas the worst-case impact shape on the end effector depends on the gripper and tool. For the limits in Table I, we assume that the human skin is similar to dew claws, as discussed in [18]. The constrained contact energies for the head are taken from [16], which already proposes conservative values. For unconstrained head contacts with pointed objects, we set the maximal contact energy to 0.077 J, which has a less than 5% chance of causing a corneal abrasion (light eye damage) according to [50].

VIII. EXPERIMENTS

This section evaluates our claims, highlighting the over-approximative nature of our energy verification regarding the given energy limits.

TABLE I
ADMISSIBLE CONTACT ENERGIES.

Body Part	Constrained Collision $T_{\text{clamp}}^{(h)}$				Unconstrained Collision $T_{\text{free}}^{(h)}$			
	Blunt [†] [J]	Wedge* [J]	Edge* [J]	Sheet* [J]	Blunt [†] [J]	Wedge [‡] [J]	Edge [‡] [J]	Sheet [‡] [J]
Hand	0.12	0.05	0.02	0.11	0.49	2.0	0.375	0.9
Lower Arm	0.325	0.05	0.02	0.11	1.3	2.0	0.375	0.9
Upper Arm	0.375	0.05	0.02	0.11	1.5	0.5	0.2	0.5
Torso and Legs	0.4	0.05	0.02	0.11	1.6	0.5	0.2	0.5
Head	0.0275 [†]	0.0275 [†]	0.0275 [†]	0.0275 [†]	0.11 [†]	0.077 [✕]	0.077 [✕]	0.077 [✕]

[†]From [16], *From [17], [‡]From [18] [✕]From [50]

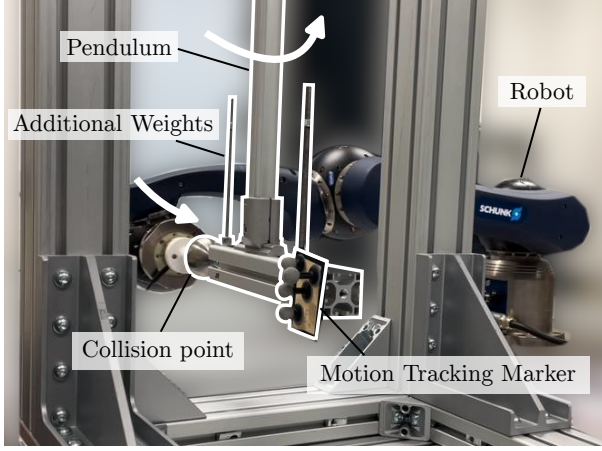


Fig. 2. The pendulum experiment setup. The robot end effector collides with the pendulum, causing it to swing backwards. A Vicon motion tracking system measures the position of the pendulum. The mass of the pendulum can be increased by adding weights to the two rods. The robot stops at the point of contact.

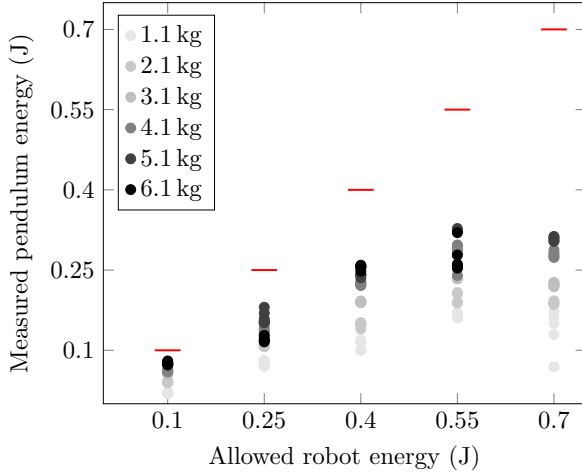


Fig. 3. Results of the kinetic energy validation using a pendulum setup for varying pendulum masses. All measured pendulum energies are below the set maximal threshold of SaRA-shield. The highest pendulum mass of 6.1 kg was left out to prevent damage to the robot hardware.

A. Kinetic energy validation

We first aim to validate that the kinetic energy of the robot is indeed below the identified energy thresholds listed in Table I. For this, we set up an experiment where the robot collides with a pendulum at different speeds, as depicted in Fig. 2.

The robot moves along a trajectory such that the normal vector of the contact is perpendicular to the rotation axis of the pendulum. The end effector and pendulum are stiff, so we assume there is an elastic collision between them. Upon collision, the pendulum swings backward, and the robot stops. We manually define the stopping point of the robot to be 5 mm behind the point of contact.

We measure the position of the pendulum with a motion-tracking system and calculate the maximum height of its center of mass in the swing-back motion using simple trigonometry. Using this measurement and the known pendulum mass, we can determine the maximum potential energy of the pendulum $T_{\text{pot}} = m_{\text{pendulum}} g \Delta z_{\text{COM}}$, where $g = 9.81 \text{ m s}^{-2}$. As the friction in the pendulum is negligible, we assume that the kinetic energy of the pendulum after the collision equals its maximal potential energy. Due to the law of conservation of energy, the kinetic energy of the robot at the time of collision never exceeds the measured potential energy of the pendulum.

In our pendulum experiment, we define the energy thresholds $T_{\text{free}}^{(h_j)} = [0.1 \text{ J}, 0.25 \text{ J}, 0.4 \text{ J}, 0.55 \text{ J}, 0.7 \text{ J}]$ of SaRA-shield and emulate a human body part j positioned at the collision point. These energy values cover the typical range of allowed contact energies in unconstrained collisions given in Table I. We chose this particular robot configuration as it allows us to reach high kinetic robot energies of up to 0.91 J. For each energy value, we let the robot collide with a pendulum of increasing mass $m_{\text{pendulum}} = [1.132 \text{ kg}, 2.132 \text{ kg}, 3.132 \text{ kg}, 4.132 \text{ kg}, 5.132 \text{ kg}, 6.132 \text{ kg}]$, with five collisions per mass value². The calculated reflected mass [28] of the robot at the collision point is 4.261 kg, so these pendulum masses cover a range including the robot mass. These masses also cover the typical effective masses of the human arm given in ISO/TS 15066:2016 [16], which are 0.6 kg for the hand, 2.6 kg for the forearm, and 5.6 kg for the entire arm.

The results in Fig. 3 show that the measured pendulum energy does not exceed the maximal allowed kinetic energy during contact for all masses. This supports our claim that SaRA-shield ensures that the kinetic energy of the robot colliding with a human is below given thresholds. For higher velocities, the measured energy was strongly below the allowed contact energy. This might indicate that our assumption of an elastic collision is incorrect. It might also indicate that the contact

²We left out the mass of 6.132 kg for the highest energy of 0.7 J to prevent damage to the robot hardware.

point at higher robot speeds was not perfectly centered on the pendulum end effector. From high-speed camera footage, we further observed that for higher robot masses, the robot occasionally hit the pendulum twice during the collision. This observation supports the claim that the measured energies are conservative.

IX. CONCLUSION

In this work, we presented SaRA-shield to ensure the safety of autonomous manipulators during active contacts with human partners. By verifying the existence of contacts with set-based reachability analysis, we achieve formal guarantees without overly restrictive robot behavior. Our contact type classification allows SaRA-shield to have significantly higher contact velocities than previous approaches, improving the overall efficiency of the framework. Our experimental evaluation shows that the robot correctly adheres to given energy constraints. Our framework is suited to provide the safety of all parts of the robot, whether sharp or blunt contacts and all human body parts. With these improvements, SaRA-shield will accelerate the deployment of autonomous agents in critical human environments.

APPENDIX A DERIVATION OF VELOCITY ERROR

In this section, we give a proof for Theorem VI.2.

Proof. The linearization error of the linear velocity $\dot{\mathbf{p}}$ projected onto an vector \mathbf{n} of an arbitrary point p on the robot in the time interval $t \in [t_0, t_0 + \Delta t]$ can be written as

$$\epsilon(t) = |\dot{\mathbf{p}}(t) \cdot \mathbf{n} - (\dot{\mathbf{p}}(t_0) + \ddot{\mathbf{p}}(t_0)(t - t_0)) \cdot \mathbf{n}|, \quad (49)$$

where $\ddot{\mathbf{p}}(t_0) = \frac{\dot{\mathbf{p}}(t_0 + \Delta t) - \dot{\mathbf{p}}(t_0)}{\Delta t}$. By approximating $v_n(t) = \dot{\mathbf{p}}(t) \cdot \mathbf{n}$ using a first-order Taylor polynomial with remainder $r_n(t, t_0)$, we can write

$$\epsilon(t) = |r_n(t, t_0)|. \quad (50)$$

The remainder term can then be limited to

$$|r_n(t, t_0)| \leq \sup_{t_0 \leq \tau \leq t_0 + \Delta t} \frac{1}{2} |\ddot{v}_n(\tau)| (t - t_0)^2. \quad (51)$$

As we know the velocity at $t = t_0$ and $t = t_0 + \Delta t$, the approximation error of the first-order Taylor polynomial is maximal at $t = t_0 + \frac{\Delta t}{2}$, so

$$\forall t \in [t_0, t_0 + \Delta t] : |r_n(t, t_0)| \leq |r_n(t_0 + \frac{\Delta t}{2}, t_0)|,$$

so we define $\epsilon_v := |r_n(t_0 + \frac{\Delta t}{2}, t_0)|$ with

$$\epsilon_v \leq \sup_{t_0 \leq \tau \leq t_0 + \Delta t} \frac{1}{8} |\ddot{v}_n(\tau)| (\Delta t)^2. \quad (52)$$

In this section, we define the vector of joint angles up to the link that contains \mathbf{p} as $\mathbf{q} \in \mathbb{R}^N$. We derive the linearization error for the positional velocity only, so we use the positional Jacobian $\mathbf{J}_P(\mathbf{q})$ that describes the contribution of the joint velocities $\dot{\mathbf{q}}$ to the linear velocity $\dot{\mathbf{p}}$. We only evaluate revolute joints and leave the derivation for prismatic joints for future

work. The projected velocity v_n can be written dependent on the joint positions and velocities

$$v_n = (\mathbf{J}_P(\mathbf{q})\dot{\mathbf{q}}) \cdot \mathbf{n} = \mathbf{J}_n(\mathbf{q})\dot{\mathbf{q}},$$

with $\mathbf{J}_n(\mathbf{q}) = \mathbf{n}^\top \mathbf{J}_P(\mathbf{q})$. So, the absolute jerk is limited to

$$|\ddot{v}_n(t)| \leq \underbrace{|\mathbf{J}_n(\mathbf{q})\ddot{\mathbf{q}}|}_{\textcircled{A}} + 2 \underbrace{|\dot{\mathbf{J}}_n(\mathbf{q}, \dot{\mathbf{q}})\dot{\mathbf{q}}|}_{\textcircled{B}} + \underbrace{|\ddot{\mathbf{J}}_n(\mathbf{q}, \dot{\mathbf{q}}, \ddot{\mathbf{q}})\dot{\mathbf{q}}|}_{\textcircled{C}}. \quad (53)$$

To derive the terms \textcircled{A} , \textcircled{B} , and \textcircled{C} , we first assume the manipulator to be an N -degree of freedom planar manipulator [48, Sec. 3.2.1] with link lengths d_i , and \mathbf{n} lying in the plane of the manipulator, so that all joints influence v_n . Without loss of generality, we assume that the point of interest \mathbf{p} lies on the outer point of the last link \mathbf{p}_N . We later show that the over-approximation derived for the planar manipulator actually over-approximates the velocity error in the general manipulator case. First, we derive $\mathbf{J}_n(\mathbf{q})$ of the planar manipulator based on the terminology of [48, Sec. 3.1]

$$\mathbf{J}_P(\mathbf{q}) = [\mathbf{J}_{P,1}, \mathbf{J}_{P,2}, \dots, \mathbf{J}_{P,N}],$$

$$\mathbf{J}_{P,k} = \mathbf{z}_{k-1} \times (\mathbf{p}_N - \mathbf{p}_{k-1}),$$

$$\mathbf{p}_0 = \begin{bmatrix} 0 \\ 0 \\ 0 \end{bmatrix}, \quad \mathbf{p}_k = \begin{bmatrix} \sum_{i=1}^k d_i \cos\left(\sum_{j=1}^i q_j\right) \\ \sum_{i=1}^k d_i \sin\left(\sum_{j=1}^i q_j\right) \\ 0 \end{bmatrix},$$

$$\mathbf{z}_k = [0 \ 0 \ 1]^\top, \quad k = 1, \dots, N$$

$$\mathbf{n} = [n_x \ n_y \ 0]^\top = [\cos(\theta_n) \ \sin(\theta_n) \ 0]^\top$$

$$\mathbf{J}_n = [\mathbf{J}_{n,1} \ \mathbf{J}_{n,2} \ \dots \ \mathbf{J}_{n,N}],$$

$$\mathbf{J}_{n,k} = \sum_{i=k}^N d_i \sin\left(\theta_n - \sum_{j=1}^i q_j\right).$$

The first- and second-order derivatives of \mathbf{J}_n with respect to time are

$$\dot{\mathbf{J}}_n = [\dot{\mathbf{J}}_{n,1} \ \dot{\mathbf{J}}_{n,2} \ \dots \ \dot{\mathbf{J}}_{n,N}],$$

$$\dot{\mathbf{J}}_{n,k} = - \sum_{i=k}^N d_i \left(\sum_{j=1}^i \dot{q}_j \right) \cos\left(\theta_n - \sum_{j=1}^i q_j\right)$$

$$\ddot{\mathbf{J}}_n = [\ddot{\mathbf{J}}_{n,1} \ \ddot{\mathbf{J}}_{n,2} \ \dots \ \ddot{\mathbf{J}}_{n,N}],$$

$$\ddot{\mathbf{J}}_{n,k} = - \sum_{i=k}^N d_i \left[\left(\sum_{j=1}^i \ddot{q}_j \right) \cos\left(\theta_n - \sum_{j=1}^i q_j\right) + \left(\sum_{j=1}^i \dot{q}_j \right)^2 \sin\left(\theta_n - \sum_{j=1}^i q_j\right) \right].$$

With this, we can approximate the terms \textcircled{A} , \textcircled{B} , and \textcircled{C} :

$$\textcircled{A} \leq \sum_{k=1}^N |\ddot{q}_k| \sum_{i=k}^N d_i \left| \cos\left(\theta_n - \sum_{j=1}^i q_j\right) \right| \quad (54)$$

$$\leq \sum_{k=1}^N |\ddot{q}_k| \sum_{i=k}^N d_i \quad (55)$$

$$\textcircled{B} \leq \sum_{k=1}^N |\ddot{q}_k| \sum_{i=k}^N d_i \sum_{j=1}^i |\dot{q}_j| \quad (56)$$

$$\textcircled{C} \leq \sum_{k=1}^N |\dot{q}_k| \sum_{i=k}^N d_i \left(\sum_{j=1}^i |\dot{q}_j| + \left(\sum_{j=1}^i |\dot{q}_j| \right)^2 \right). \quad (57)$$

Inserting (54) - (57) into (53) and (53) into (52) gives us the linearization error in (27). By over-approximating $\left| \sin \left(\theta_n - \sum_{j=1}^i q_j \right) \right| \leq 1$ and $\left| \cos \left(\theta_n - \sum_{j=1}^i q_j \right) \right| \leq 1$, we assume that the rotation axis of each joint is orthogonal to \mathbf{n} , thereby having maximal impact to the velocity of \mathbf{p} in the direction of \mathbf{n} . The over-approximations derived above are, therefore, also valid for the general manipulator case. \square

ACKNOWLEDGMENT

The authors gratefully acknowledge financial support by the Horizon 2020 EU Framework Project CONCERT under grant 101016007 and financial support by the DAAD program Konrad Zuse Schools of Excellence in Artificial Intelligence, sponsored by the Federal Ministry of Education and Research.

REFERENCES

- [1] J. Trevelyan, W. R. Hamel, and S.-C. Kang, "Robotics in hazardous applications," in *Springer Handbook of Robotics*, B. Siciliano and O. Khatib, Eds. Springer International Publishing, 2016, pp. 1521–1548.
- [2] J. Smids, S. Nyholm, and H. Berkers, "Robots in the workplace: A threat to—or opportunity for—meaningful work?" *Philosophy & Technology*, vol. 33, no. 3, pp. 503–522, 2020.
- [3] I. Research, "Size of the market for industrial robots worldwide from 2018 to 2020, with a forecast through 2028 (in billion u.s. dollars)." Statista, Tech. Rep., 2021.
- [4] Statista, "Industry 4.0: In-depth market analysis," Tech. Rep., 2023.
- [5] K. Suita, Y. Yamada, N. Tsuchida, K. Imai, H. Ikeda, and N. Sugimoto, "A failure-to-safety "kyozon" system with simple contact detection and stop capabilities for safe human-autonomous robot coexistence," in *Proc. of the IEEE Int. Conf. on Robotics and Automation (ICRA)*, vol. 3, 1995, pp. 3089–3096.
- [6] K. Kokkalis, G. Michalos, P. Aivaliotis, and S. Makris, "An approach for implementing power and force limiting in sensorless industrial robots," *Procedia CIRP*, vol. 76, pp. 138–143, 2018.
- [7] P. Svarny, M. Tesar, J. K. Behrens, and M. Hoffmann, "Safe physical hri: Toward a unified treatment of speed and separation monitoring together with power and force limiting," in *Proc. of the IEEE/RSJ Int. Conf. on Intelligent Robots and Systems (IROS)*, 2019, pp. 7580–7587.
- [8] N. Lucci, B. Lacevic, A. M. Zanchettin, and P. Rocco, "Combining speed and separation monitoring with power and force limiting for safe collaborative robotics applications," *IEEE Robotics and Automation Letters*, vol. 5, no. 4, pp. 6121–6128, 2020.
- [9] S. Ergun, Y. Ding, H. Alagi, C. Schöffmann, B. Ubezio, G. Soti, M. Rathmair, S. Mühlbacher-Karrer, U. Thomas,

- B. Hein, M. Hofbaur, and H. Zangl, "A unified perception benchmark for capacitive proximity sensing towards safe human-robot collaboration (hrc)," in *Proc. of the IEEE Int. Conf. on Robotics and Automation (ICRA)*, 2021, pp. 3634–3640.
- [10] T. Steinecker, A. Kurdas, N. Mansfeld, M. Hamad, R. J. Kirschner, S. Abdolshah, and S. Haddadin, "Mean reflected mass: A physically interpretable metric for safety assessment and posture optimization in human-robot interaction," in *Proc. of the IEEE Int. Conf. on Robotics and Automation (ICRA)*, 2022, pp. 11 209–11 215.
- [11] S. Haddadin, S. Haddadin, A. Khoury, T. Rokahr, S. Parusel, R. Burgkart, A. Bicchi, and A. Albu-Schäffer, "On making robots understand safety: Embedding injury knowledge into control," *The International Journal of Robotics Research*, vol. 31, no. 13, pp. 1578–1602, 2012.
- [12] D. Beckert, A. Pereira, and M. Althoff, "Online verification of multiple safety criteria for a robot trajectory," in *Proc. of the IEEE Conf. on Decision and Control (CDC)*, 2017, pp. 6454–6461.
- [13] S. B. Liu and M. Althoff, "Online verification of impact-force-limiting control for physical human-robot interaction," in *Proc. of the IEEE/RSJ Int. Conf. on Intelligent Robots and Systems (IROS)*, 2021, pp. 777–783.
- [14] J. Lachner, F. Allmendinger, E. Hobert, N. Hogan, and S. Stramigioli, "Energy budgets for coordinate invariant robot control in physical human–robot interaction," *The International Journal of Robotics Research*, vol. 40, no. 8-9, pp. 968–985, 2021.
- [15] ISO, "Robotics - safety requirements - part 1: Industrial robots," International Organization for Standardization, Tech. Rep. DIN EN ISO 10218-1:2021-09 DC, 2021.
- [16] —, "Robots and robotic devices - collaborative robots," International Organization for Standardization, Tech. Rep. ISO/TS 15066:2016(E), 2016.
- [17] R. J. Kirschner, C. M. Micheler, Y. Zhou, S. Siegner, M. Hamad, C. Glowalla, J. Neumann, N. Rajaei, R. Burgkart, and S. Haddadin, "Towards safe robot use with edged or pointed objects: A surrogate study assembling a human hand injury protection database," in *Proc. of the IEEE Int. Conf. on Robotics and Automation (ICRA)*, 2024.
- [18] R. J. Kirschner, J. Yang, E. Elshani, C. M. Micheler, T. Leibbrand, D. Müller, C. Glowalla, N. Rajaei, R. Burgkart, and S. Haddadin, "Towards unconstrained collision injury protection data sets: Initial surrogate experiments for the human hand," 2024. [Online]. Available: <http://arxiv.org/abs/2408.06175>
- [19] J. Thumm and M. Althoff, "Provably safe deep reinforcement learning for robotic manipulation in human environments," in *Proc. of the IEEE Int. Conf. on Robotics and Automation (ICRA)*, 2022, pp. 6344–6350.
- [20] J. A. Marvel and R. Norcross, "Implementing speed and separation monitoring in collaborative robot work-cells," *Robotics and computer-integrated manufacturing*, vol. 44, pp. 144–155, 2017.
- [21] B. Lacevic, A. M. Zanchettin, and P. Rocco, "Towards

- the exact solution for speed and separation monitoring for improved human-robot collaboration,” in *Proc. of the IEEE Int. Symp. on Robot and Human Interactive Communication (ROMAN)*, 2020, pp. 1190–1195.
- [22] A. Pereira and M. Althoff, “Overapproximative human arm occupancy prediction for collision avoidance,” *IEEE Transactions on Automation Science and Engineering*, vol. 15, no. 2, pp. 818–831, 2018.
- [23] M. Althoff, A. Giusti, S. B. Liu, and A. Pereira, “Effortless creation of safe robots from modules through self-programming and self-verification,” *Science Robotics*, vol. 4, no. 31, pp. 1–14, 2019.
- [24] S. Schepp, J. Thumm, S. B. Liu, and M. Althoff, “SaRA: A tool for safe human–robot coexistence and collaboration through reachability analysis,” in *Proc. of the IEEE Int. Conf. on Robotics and Automation (ICRA)*, 2022, pp. 4312–4317.
- [25] S. Haddadin, A. Albu-Schäffer, and G. Hirzinger, “Requirements for safe robots: Measurements, analysis and new insights,” *The International Journal of Robotics Research*, vol. 28, no. 11-12, pp. 1507–1527, 2009.
- [26] R. J. Kirschner, N. Mansfeld, S. Abdolshah, and S. Haddadin, “Experimental analysis of impact forces in constrained collisions according to ISO/ts 15066,” in *IEEE Int. Conf. on Intelligence and Safety for Robotics (ISR)*, 2021, pp. 1–5.
- [27] R. J. Kirschner, N. Mansfeld, G. G. Peña, S. Abdolshah, and S. Haddadin, “Notion on the correct use of the robot effective mass in the safety context and comments on ISO/ts 15066,” in *IEEE Int. Conf. on Intelligence and Safety for Robotics (ISR)*, 2021, pp. 6–9.
- [28] O. Khatib, “Inertial properties in robotic manipulation: An object-level framework,” *The International Journal of Robotics Research*, vol. 14, no. 1, pp. 19–36, 1995.
- [29] C. Sloth and H. G. Petersen, “Computation of safe path velocity for collaborative robots,” in *Proc. of the IEEE/RSJ Int. Conf. on Intelligent Robots and Systems (IROS)*, 2018, pp. 6142–6148.
- [30] P. Aivaliotis, S. Aivaliotis, C. Gkournelos, K. Kokkalis, G. Michalos, and S. Makris, “Power and force limiting on industrial robots for human-robot collaboration,” *Robotics and Computer-Integrated Manufacturing*, vol. 59, pp. 346–360, 2019.
- [31] A. Golshani, A. Kouhkord, A. Ghanbarzadeh, and E. Najafi, “Control design for safe human-robot collaboration based on ISO/ts 15066 with power and force limit,” in *2023 11th RSI International Conference on Robotics and Mechatronics (ICRoM)*, 2023, pp. 279–284.
- [32] M. Hamad, A. Kurdas, N. Mansfeld, S. Abdolshah, and S. Haddadin, “Modularize-and-conquer: A generalized impact dynamics and safe precollision control framework for floating-base tree-like robots,” *IEEE Transactions on Robotics*, pp. 1–22, 2023.
- [33] A. Pupa, M. Minelli, and C. Secchi, “A time-optimal energy planner for safe human-robot collaboration,” in *Proc. of the IEEE Int. Conf. on Robotics and Automation (ICRA)*, 2024, pp. 17 373–17 379.
- [34] W. Eisenmenger, “Spitze, scharfe und halbscharfe gewalt,” in *Handbuch Gerichtliche Medizin*. Springer Berlin, 2004, vol. 1, pp. 571–592.
- [35] B. Povse, D. Koritnik, T. Bajd, and M. Munih, “Correlation between impact-energy density and pain intensity during robot-man collision,” in *2010 3rd IEEE RAS & EMBS International Conference on Biomedical Robotics and Biomechanics*, 2010, pp. 179–183.
- [36] R. Behrens and N. Elkmann, “Study on meaningful and verified thresholds for minimizing the consequences of human-robot collisions,” in *Proc. of the IEEE Int. Conf. on Robotics and Automation (ICRA)*, 2014, pp. 3378–3383.
- [37] R. Behrens, G. Pliske, S. Piatek, F. Walcher, and N. Elkmann, “A statistical model to predict the occurrence of blunt impact injuries on the human hand-arm system,” *Journal of Biomechanics*, vol. 151, 2023.
- [38] Y. Yamada, Y. Hirasawa, S. Huang, and Y. Umetani, “Fail-safe human/robot contact in the safety space,” in *Proceedings 5th IEEE International Workshop on Robot and Human Communication. RO-MAN’96 TSUKUBA*, 1996, pp. 59–64.
- [39] U. Asad, S. Rasheed, W. A. Lughmani, T. Kazim, A. Khalid, and J. Pannek, “Biomechanical modeling of human–robot accident scenarios: A computational assessment for heavy-payload-capacity robots,” *Applied Sciences*, vol. 13, no. 3, 2023.
- [40] ISO, “Safety of machinery - positioning of safeguards with respect to the approach speeds of parts of the human body,” International Organization for Standardization, Tech. Rep. DIN EN ISO 13855:2010-10 ST N, 2010.
- [41] S. Kumar, S. Arora, and F. Sahin, “Speed and separation monitoring using on-robot time-of-flight laser-ranging sensor arrays,” in *IEEE Int. Conf. on Automation Science and Engineering (CASE)*, 2019, pp. 1684–1691.
- [42] U. B. Himmelsbach, T. M. Wendt, and M. Lai, “Towards safe speed and separation monitoring in human-robot collaboration with 3D-time-of-flight cameras,” in *Proc. of the IEEE Int. Conf. on Robotic Computing (IRC)*, 2018, pp. 197–200.
- [43] M. J. Rosenstrauch, T. J. Pannen, and J. Krüger, “Human robot collaboration - using kinect v2 for ISO/ts 15066 speed and separation monitoring,” *Procedia CIRP*, vol. 76, pp. 183–186, 2018.
- [44] B. Yang, S. Xie, G. Chen, Z. Ding, and Z. Wang, “Dynamic speed and separation monitoring based on scene semantic information,” *Journal of Intelligent & Robotic Systems*, vol. 106, no. 2, 2022.
- [45] S. Fujii and Q.-C. Pham, “Real-time batched distance computation for time-optimal safe path tracking,” in *Proc. of the IEEE Int. Conf. on Robotics and Automation (ICRA)*, 2024, pp. 13 383–13 389.
- [46] S. B. Liu, B. Schürmann, and M. Althoff, “Guarantees for real robotic systems: Unifying formal controller synthesis and reachset-conformant identification,” *IEEE Transactions on Robotics (Early Access)*, pp. 1–15, 2023.
- [47] S. Bi, C. Yuan, C. Liu, J. Cheng, W. Wang, and Y. Cai, “A survey of low-cost 3D laser scanning technology,” *Applied Sciences*, vol. 11, no. 9, 2021.

- [48] B. Siciliano, L. Sciavicco, L. Villani, and G. Oriolo, *Robotics: Modelling, Planning and Control*, M. J. Grizzle and M. A. Johnson, Eds. Springer, 2009.
- [49] DIN, “Ergonomics – human body dimensions – part 2: Values,” Deutsches Institut für Normung e. V. (DIN), Tech. Rep. DIN 33402-2:2020-12, 2020.
- [50] S. M. Duma, T. P. Ng, E. A. Kennedy, J. D. Stitzel, I. P. Herring, and F. Kuhn, “Determination of significant parameters for eye injury risk from projectiles,” *Journal of Trauma and Acute Care Surgery*, vol. 59, no. 4, 2005.